JOURNAL OF CATALYSIS 146, 394–406 (1994)

NO–CO Activity and Selectivity over a $Pt_{10}Rh_{90}(111)$ Alloy Catalyst in the 10-Torr Pressure Range

K. Y. Simon Ng,[1] David N. Belton,[2] Steven J. Schmieg, and Galen B. Fisher

General Motors Research and Development Center, Physical Chemistry Department, Building 1-6, 30500 Mound Road, Box 9055, Warren, Michigan 48090-9055

Received August 13, 1993; revised October 25, 1993

We have studied the effects of temperature, NO conversion, and NO–CO ratio on the activity and selectivity of the NO–CO reaction over a $Pt_{10}Rh_{90}(111)$ surface. The NO–CO activity over the $Pt_{10}Rh_{90}(111)$ is very similar to that over the Rh(111) surface from 573 to 648 K in that both surfaces have the same E_a, reaction orders, products, and selectivities. The turnover numbers for the $Pt_{10}Rh_{90}(111)$ alloy are slightly lower than those for Rh(111), when compared on a *per surface atom* basis; however, the rates per surface Rh atom are virtually unchanged. This behavior suggests that the primary effect of Pt is to dilute the Rh surface atom concentration; however, it is equally consistent with electronic modification of all surface atoms. The surface composition remains essentially unchanged over the range of reaction conditions that we explored; however, we did not go extremely oxidizing, which is the condition known to have the largest effect on the surface composition. The $Pt_{10}Rh_{90}(111)$ single crystal mimics the behavior of supported Pt–Rh catalysts in that both show high (~75%) selectivity for N_2O at low temperature, low conversion, or high NO–CO ratio and low or zero N_2O production at high temperature and high NO conversion. Our conclusion is that the N_2O selectivity and the overall reaction rate are controlled by the NO adsorption/desorption equilibrium. Adsorbed NO strongly inhibits the NO dissociation reaction, keeping surface N coverages low. However, once the temperature is raised or the NO pressure lowered, surface NO coverages fall, accelerating the NO dissociation reaction and likewise increasing the N + N reaction. We conclude that these surface kinetics explain the curious N_2O selectivities observed during light-off of supported catalysts.

1. INTRODUCTION

Platinum and rhodium are widely used in the current generation of automotive catalytic converters because of their unique catalytic activity and durability in automotive exhaust (1, 2). Both platinum and rhodium are very effective at oxidizing CO to CO_2, but it is generally believed that Pt is superior for hydrocarbon (HC) oxidation, with Rh being best for NO reduction. Beginning in 1994, government regulations mandate that vehicle emissions for both HC and NO must fall substantially from current levels. Thus, there are increasing efforts to achieve better activity from both Pt and Rh in automotive catalysts. These tougher U.S. standards are being implemented at a time when the rest of the world, primarily Europe, is adopting regulations that will effectively double the number of vehicles worldwide which are equipped with a catalytic converter. This combination of tougher U.S. standards and increased European usage has the potential to strain the world's Rh supplies. Given these strong pressures on noble metal supply, it is imperative that Rh and Pt be utilized as effective as possible for the control of automotive emissions; one part of our effort is focused on obtaining a more detailed understanding of the reactivity of these vital catalyst components. To this end we have a continuing program to define and understand the reaction kinetics over well-defined single-crystal catalysts under conditions of temperature and pressure comparable to those encountered in automotive exhaust. By studying such well-defined model catalysts we are able to isolate the activity of the noble metal component of the catalyst free from complicating factors such as metal particle size and catalyst support effects. Because single crystals have well-defined surface areas and no support effects, they are ideal for activity comparisons between different metals and metal alloys.

The experiments presented here examine the NO–CO activity of a $Pt_{10}Rh_{90}(111)$ alloy single crystal. Our interest in Pt–Rh alloys stems from recent reports that in actual catalytic converters the majority of the noble metal particles exist as multimetallic particles (3). In this paper we examine the activity of a Pt/Rh alloy crystal with primarily three questions in mind. First, we wish to probe the effect of adding Pt, which is less active for NO reduction, to the more active Rh component. Single crystals are especially suitable for making this type of comparison because the

[1] On leave from Department of Chemical Engineering, Wayne State University, Detroit, MI 48202.

[2] To whom correspondence should be addressed.

0021-9517/94 $6.00

number of surface or active metal atoms is well defined; therefore, no ambiguities from estimating active metal surface area are introduced into the comparison with the Rh-only catalyst. Another advantage that single crystals offer for an experiment of this kind is that by using surface analysis we can very precisely define both the surface and the bulk Pt and Rh concentrations. For the experiments presented here we know that Pt is enriched at the surface relative to the bulk, making the surface concentration of our catalyst approximately Pt_{30} Rh_{70} (4, 5). We have also already determined in ultrahigh vacuum (UHV) surface science that the $Pt_{10}Rh_{90}(111)$ alloy behaves as if it has "averaged" surface electronic properties for oxygen desorption (5) and NO dissociation (6). Second, we wish to contrast the activity and selectivity of the Pt–Rh single crystal to those reported for supported Pt–Rh catalysts. When CO and NO are reacted over supported Pt–Rh catalysts, the N_2O selectivity is a strong function of reaction temperature and/or NO conversion (7). This tendency to form N_2O under laboratory conditions is quite different from what is observed in engine exhaust, where it has been reported that very little N_2O is actually produced (8). Understanding the kinetics which lead to N_2O vs N_2 formation is quite important, considering that N_2 is the desired product from catalytic converters on cars.

Finally, we are interested in making more complex comparisons of single-crystal and supported catalyst reactivities. Kinetic measurements over single-crystal catalysts are important primarily because they offer the best systems for detailed understanding of reaction kinetics and mechanisms. This statement is true primarily because single crystals are amenable to measurements of the rates of individual or elementary steps in the mechanism. Without measurements of the rates of at least some of the elementary steps it is virtually impossible to verify/eliminate a given reaction mechanism. Although single crystals clearly cannot reproduce the activity of supported systems under all conditions, there is ample evidence that for simple feeds ($CO–O_2$) over monometallic catalysts, supported and single-crystal catalysts have very similar activity (9). We have already studied the NO–CO and $CO–N_2O$ (11) reactions over Rh(111) in the same apparatus. In our previous paper (10), we showed that N_2O is the major N-containing product of the NO–CO reaction over Rh(111) over a wide range of pressures above 2 Torr. The paper by Belton and Schmieg (10) showed that earlier work over Rh(111) (9) correctly measured the overall reaction rate (CO_2 formation rate) but was incomplete in that it was unable to detect the nitrogen-containing products (N_2O formation was not addressed). In this paper we examine a more complicated bimetallic catalyst, Pt–Rh, and a reaction, NO–CO, that exhibits rather complicated kinetics. In a parallel study, we have examined the $CO–O_2$ and $CO–N_2O$ activities on the same Pt–Rh alloy surface (12).

There have been a number of papers on the NO–CO reaction at pressures around 10 Torr over supported Rh (13–18) and Pt–Rh (7, 19, 20) catalysts, in addition to several papers on Rh (21–26) and Pt–Rh (27, 28) single-crystal catalysts. Most of the moderate pressure kinetic data to date over Pt–Rh alloy single crystals are for the $NO–H_2$ reaction (29), which we do not address here. Over supported Rh, supported Pt–Rh, and Rh single-crystal catalysts, there is now general agreement as to the kinetics and selectivities at low temperatures and/or low NO conversion. Over all of these catalysts it is reported that N_2O is the primary N-containing product, the apparent activation energy (above 480 K) is between 33 and 38 kcal/mol, and the reaction rate and selectivity are roughly independent of both the CO and the NO pressures (between 1 and 100 Torr). In contrast, the behaviors of these catalysts appear to be different at higher temperatures and/or NO conversions. Whereas Rh(111) (10) and 5 wt% Rh/SiO_2 (13) make less N_2O at high temperature than at lower temperature, N_2O remains the primary product. On the other hand, Rh/Al_2O_3 (16–18) and $Pt/Rh/Al_2O_3$ (19, 20) catalysts produced almost exclusively N_2 at high temperatures and NO conversions. Understanding these very interesting variations in kinetics is in part the motivation for this work.

In this paper we report that addition of Pt to a Rh surface has primarily a dilution effect on the Rh activity. Whether this occurs locally or by an averaged electronic effect is difficult to distinguish. Substitution of 30% of the Rh surface atoms by Pt atoms lowers the specific rates for all of the reaction products (CO_2, N_2O, and N_2) by about 35%. The selectivity behavior of this $Pt_{10}Rh_{90}(111)$ alloy is quite similar to that reported for a 1 wt% Pt/0.2% Rh/Al_2O_3-supported catalyst (7) for N_2O formation. These results suggest that formation of alloy particles of Pt and Rh in supported catalysts has primarily the effect of lowering the activity of the Rh component. As for the reaction kinetics, our results suggest that the important surface phenomenon for controlling the selectivity of the reaction is the NO adsorption/desorption equilibrium.

2. EXPERIMENTAL

2.1. Apparatus

The experiments were performed in a custom-built system that couples a UHV analysis chamber to a moderate-pressure (<100 Torr) reactor. The reactor and analysis chamber are separated with a gate valve. The UHV analysis chamber is equipped with a wide array of surface analytical techniques. For this study we used Auger electron spectroscopy (AES), X-ray photoelectron spectroscopy (XPS), and low-energy electron diffraction

(LEED). The gases used in these experiments were 99.0% NO and 99.99% CO (Scott Specialty Gases). The NO had <0.15% N_2O and <0.5% N_2 contamination, while the CO was in an Al cylinder and was trapped with a liquid nitrogen bath to exclude any metal carbonyls from the reactor. The gases were leaked into the reactor at low pressure, as measured by a baratron gauge. The reactor has a volume of 0.756 liter and is pumped with a turbomolecular pump with an ultimate base pressure of 10^{-9} Torr. The pump is separated from the reactor with a gate valve. A Ta evaporator was attached to a miniconflat port on the side of the reactor and consisted of a 0.015-in. etched Ta wire spot welded to a 0.125-in. Ta post connected to a 15-A electrical feedthrough. The wire was ~25 mm from the sample during evaporation. The sample could be transferred from the reactor to the UHV analysis chamber within 5 min after reactor pumpdown, with a typical base pressure of 10^{-9} Torr during spectroscopic analysis.

2.2. Sample Preparation

The Pt–Rh sample was obtained from a boule of $Pt_{10}Rh_{90}$ oriented along the [111] direction. The crystal was cut so that both sides of the sample were oriented to ±0.5 degree of the (111) plane as shown by the Laue diffraction pattern. The sample was sanded and polished with diamond paste, with the final polish being 0.25-μm grit. The Pt–Rh sample was elliptical (~5 × ~10 mm) wth an area of ~0.4 cm^2 per side and a thickness of ~1 mm. The number of active sites (including both Pt and Rh) was calculated to be 1.25×10^{15} (both sides).

The cleaning procedure consisted of flowing 99.9999% H_2 over the sample in a quartz tube furnace for 4 days at 1275 K and 1 day at 1075 K. This procedure has been shown to be effective at removing any low-Z impurities from the bulk, such as C, B, P, and Si. The sample was then repolished with 0.25-μm diamond paste to remove residues which may have been deposited on the surface during the furnace treatment. After polishing, the sample was etched in hot HF : HNO_3 (3 : 1) for several minutes. The sample was mounted on a transfer device using four etched 0.015-in. Ta wires spot welded to the back of the sample for resistive heating. A 0.003-in. chromel–alumel thermocouple was also spot welded to the back of the sample to monitor the crystal temperature. After mounting, the sample was rinsed with HNO_3 to remove spot welding residue, followed by rinsing with distilled H_2O and methanol.

2.3. Sample Cleaning

A sharp (1 × 1) LEED pattern was obtained on the front of the sample by Ar^+ sputtering (2 keV, ~12 μA) for ~32 hr with the sample at 875 K, followed by annealing at 1425 K for 10 min. This extensive sputtering treatment was necessary to obtain a sharp LEED pattern and has been successful in ordering Rh single-crystal surfaces. Sputtering removed all surface contamination and yielded a surface concentration that was the same as the bulk, $Pt_{10}Rh_{90}$, while the annealing treatment resulted in a stable Pt surface concentration of 31% (±5%). The surface cleanliness was monitored with XPS, while the surface cleanliness and composition were monitored with AES. The surface order was periodically checked with LEED.

2.4. Gas Chromatography Measurements

Reactions were done in a batch mode. All products and reactants were measured with a Varian 3400 gas chromatograph (GC) using simultaneous injection of sample (2 × 250 μl) into each of two columns operated at 313 K with a He carrier gas. Column effluents were monitored using both a thermal conductivity detector (TCD) and a flame ionization detector (FID). Gases passed first through the TCD, then through a methanizer with a Ni catalyst, and then to the FID. The TCD filament temperature was maintained at 573 K, the methanizer temperature at 658 K, and the detector temperature at 423 K. Using this arrangement we were able to detect N_2 (TCD), NO (TCD), CO (FID), CO_2 (TCD), and N_2O (TCD). One sample entered a molecular sieve column, where N_2, NO, and CO were separated before passing on to the detectors for analysis. The other sample entered a delay column followed by a Hayesep DIP column which delayed entry and subsequent elution of components from the Hayesep DIP column until the last molecular sieve component (CO) eluted. At this point a valve was switched to direct the Hayesep DIP effluent to the detectors for the measurement of CO_2 and N_2O. The experimental procedure for making a rate measurement was as follows: (i) the gate valves to the UHV analysis chamber and the reactor turbomolecular pump were closed, (ii) the reactants were leaked into the reactor, (iii) the sample was ramped to the reaction temperature at approximately 15 K/sec, (iv) the timer was started when the sample was within 5° of the reaction temperature, (v) the temperature was held (±2°) for a specified time interval, (vi) the sample was cooled to room temperature, and (vii) the gases in the reactor were expanded into the evacuated GC sampling loops.

2.5. Tantalum Evaporation

Ta was used to cover the back of the sample because (i) the back already contained the Ta heating leads and thermocouple, (ii) Ta oxide showed no activity for the reaction studied, and (iii) it allowed us to characterize only one side of the sample spectroscopically. Evaporation of Ta was performed by passing ~12 A of current through the Ta wire for 20 min, which was sufficient to cover the

back of the sample with ~50 Å of Ta. XPS was used to calculate the Ta oxide thickness by (i) assuming that a uniform Ta oxide layer was deposited, (ii) measuring the attenuation of the Rh($3d_{5/2}$) peak, and (iii) using a 15-Å escape length for the Rh(3*d*) electrons. AES showed no Rh or Pt on the surface, only Ta and oxygen. Sulfur and carbon contamination deposited on the front of the sample during Ta evaporation was easily removed by oxidation during reaction with 8 Torr of O_2 and 8 Torr of CO at 548 K. This treatment also more completely oxidized the Ta, although the surface was mostly oxidized during evaporation due to background H_2O in the reactor. Ta could be removed by annealing the sample at 1425 K for 10 min due either to diffusion into bulk or to evaporation. The rate and selectivity for the NO–CO reaction were measured prior to Ta evaporation to ensure that the Ta showed no catalytic activity and had no effect on the product distribution. Ta oxide blocks the Pt–Rh sites on the back of the sample since the rate of the front and the back is twice the rate of the front with Ta oxide on the back. The activation energy and selectivity were unchanged.

2.6. *Surface Composition of $Pt_{10}Rh_{90}(111)$*

The surface composition of this particular Pt–Rh alloy single crystal was previously studied in great detail using a combination of ion scattering spectroscopy (ISS), and AES (4). In (4) it was shown that, under the conditions applicable to this paper, AES (corrected for Pt and Rh relative AES cross-sections) is a reliable indicator of the surface composition. In agreement with previous papers (4, 5) we determined that after the $Pt_{10}Rh_{90}$ surface was sputtered at room temperature for 30 min with Ar^+ at 2 keV/12 μA the Pt concentration was almost exactly 10%, which is the bulk concentration. After the room temperature sputtering, the Pt–Rh alloy was then annealed at 1425 K for 10 min and AES data were taken. At this point, AES showed that the Pt surface concentration had increased to 31% (±5%). This result is also in complete agreement with the previously reported Pt–Rh alloy behavior. Based on these two endpoints, we feel confident that we can rely on the previous AES/ISS calibrations to define the surface Pt and Rh concentrations.

Next the sample was placed in the moderate-pressure reactor with 8 Torr CO/8 Torr of NO, and the reaction was run at 623 K for 5 min. After this treatment the sample was returned to the UHV system, and AES spectra were obtained without any further heating of the sample. After the reaction AES indicated that the Pt concentration had dropped from 31% to about 22%. Next the crystal was flashed to 875 K to desorb NO and N from the surface. After the flash to 875 K, the Pt concentration, as measured by AES, increased to 28%. Based on previous, very extensive ISS/AES studies we do not expect the surface Pt concentration to change during this relatively low-temperature, postreaction anneal. Therefore, we conclude that the true surface Pt concentration is 28% during reaction and does not change significantly, as during our experiments. At this time we are investigating the apparent preferential screening effects that give anomalously low surface Pt concentrations after the NO–CO reaction.

3. RESULTS

3.1. *NO–CO Activity*

Figure 1 shows the turnover number (TON) for CO_2, N_2O, and N_2 formation plotted in an Arrhenius fashion as a function of inverse temperature. The data (Fig. 1) were obtained by reacting 8 Torr NO and 8 Torr CO (8/8) over the $Pt_{10}Rh_{90}(111)$ crystal. In the temperature range represented in Fig. 1 (573 to 698 K), the three products (CO_2, N_2O, and N_2) are formed with apparent activation energies, E_a, of 31.2, 30.9, and 32.8 kcal/mol, respectively, when the data are analyzed using an Arrhenius equation. The corresponding preexponential factors (ν) are 4.6×10^{12}, 2.4×10^{12}, and 3.2×10^{12} site^{-1} sec^{-1}. For the experiments in Fig. 1 the data are obtained only over that temperature range for which we could accurately measure TONs—which means that the reaction time is greater than 30 sec—while keeping the overall NO conversion below 12%.

In Fig. 2 we show a direct comparison of the CO_2 TONs for reaction of NO and CO (8/8) over both Rh(111) and $Pt_{10}Rh_{90}(111)$. For simplicity, only the CO_2 TONs are plot-

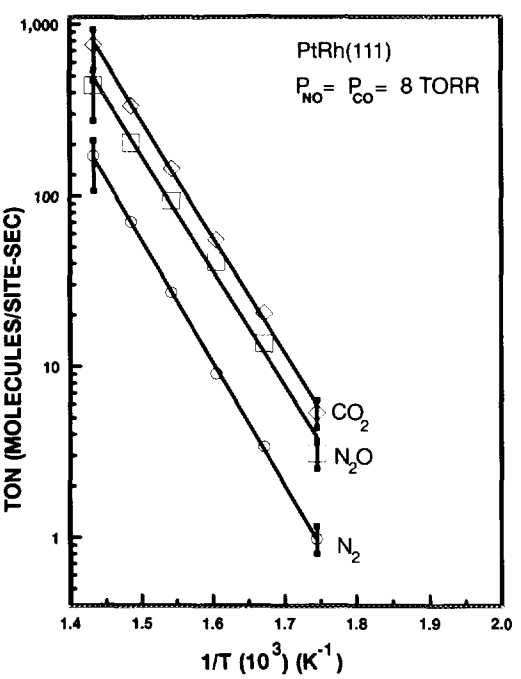

FIG. 1. Specific rates of CO_2, N_2O, and N_2 formation for the NO–CO reaction over $Pt_{10}Rh_{90}(111)$ as a function of inverse temperature.

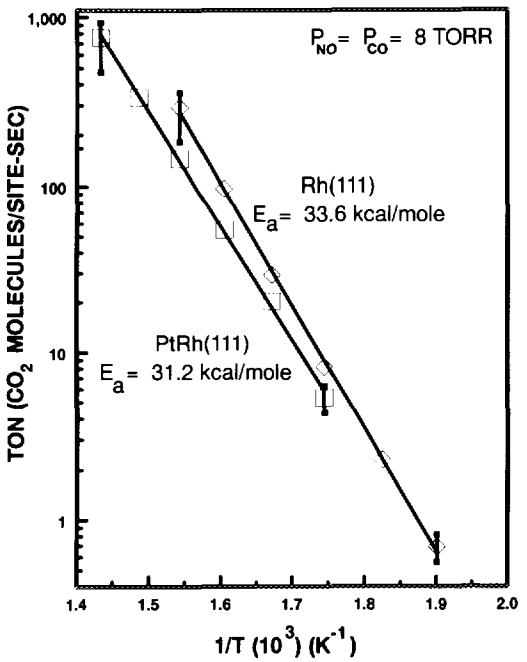

FIG. 2. Comparison of specific rates of CO_2 formation for the CO + NO reaction over $Pt_{10}Rh_{90}(111)$ and Rh(111) [5a] as a function of inverse temperature. Both surfaces have similar TONs and apparent activation energies.

ted; however, exactly the same trends are observed for both N_2O and N_2 formation rates. The Rh(111) data were measured in previous experiments (10) in the same reactor using the same experimental method as that used to measure the $Pt_{10}Rh_{90}(111)$ reaction rates. However, after the Rh(111) data were obtained but before the $Pt_{10}Rh_{90}(111)$ measurements were made, the GC was upgraded to allow for separation and detection of N_2. For the Rh(111) the N_2 formation rates were calculated from the known stoichiometry of the reaction and the measured N_2O and CO_2 formation rates (10). In Table 1 the activation energies and preexponential factors for CO_2, N_2O, and N_2 formation over both Rh(111) and $Pt_{10}Rh_{90}(111)$ are given. The Table 1 data show that Rh(111) exhibits a slightly higher activation energy and preexponential factor for formation of all three products than does the $Pt_{10}Rh_{90}(111)$ surface. These differences fall just within the largest possible error limits expected in our measurements, which suggests that there may be a small E_a difference for the reaction over these two different surfaces. As for the specific rates, taking CO_2 as the measure of the overall reaction rate we find that the $Pt_{10}Rh_{90}(111)$ TONs—activity on a per surface atom basis (not per surface Rh atom)—are between 35 and 50% lower than the Rh(111) TONs over the temperature range where data for both crystals exist.

Figure 3 shows the effect of NO pressure on the NO–CO reaction rate over $Pt_{10}Rh_{90}(111)$ at two different

TABLE 1

Apparent Activation Energies and Frequency Factors for CO_2, N_2O, and N_2 for the NO–CO Reaction over $Pt_{10}Rh_{90}(111)$ and Rh(111)

P_{NO} = P_{CO} = 8 Torr	CO_2	N_2O	N_2
Rh(111)			
E_a[a]	33.6	34.1	32.8
ν[b]	6.0×10^{13}	5.3×10^{13}	6.6×10^{12}
PtRh(111)			
E_a[a]	31.2	30.9	32.8
ν[b]	4.6×10^{12}	2.4×10^{12}	3.2×10^{12}

[a] kcal/mol.
[b] Molecules/site-sec.

temperatures (623 and 698 K). The CO pressure was kept constant at 8 Torr, and the NO pressure was varied from 2 to 40 Torr. Figure 3 shows that, within experimental error, the CO_2, N_2O, and N_2 TONs are invariant with NO pressure over the NO pressure range examined. Thus, the NO–CO reaction has an apparent zero-order dependence on the NO pressure. A similar experiment was performed to obtain the CO reaction order. Figure 4 shows the reaction rate data obtained with the NO pressure constant at 8 Torr and the CO pressure varied from 2 to 40 Torr, at T = 623 and 698 K. As in the NO reaction-order dependency, the TONs of CO_2, N_2O, and N_2 are not

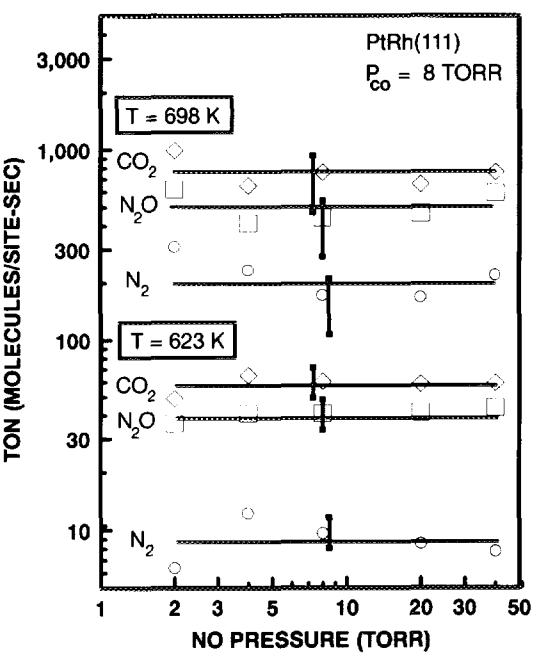

FIG. 3. The CO_2, N_2O, and N_2 TONs as a function of NO pressure with a fixed CO pressure of 8 Torr at 623 and 698 K over $Pt_{10}Rh_{90}(111)$. The data show that the production of all three products has an apparent zero order dependence on NO pressure.

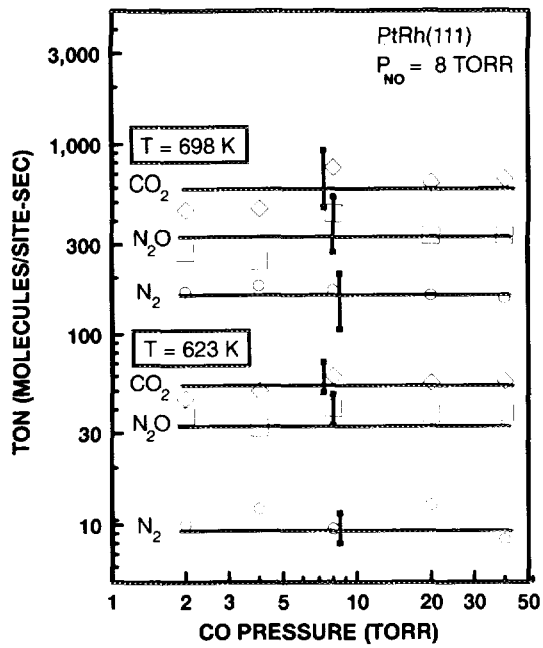

FIG. 4. The CO_2, N_2O, and N_2 TONs as a function of CO pressure with a fixed NO pressure of 8 Torr at 623 and 698 K over $Pt_{10}Rh_{90}(111)$. The data show that the production of all three products has an apparent zero order dependence on CO pressure.

sensitive to the change of CO pressure over the pressure range studied. Thus, the NO–CO reaction also has an apparent zero-order dependence on the CO pressure.

3.2. N_2O Selectivity

The selectivity of N_2O [defined as moles of N_2O/(moles of N_2O + moles of N_2)] is found to be centered around 80% in all the experiments described above. However, those experiments were performed at temperatures between 573 and 698 K with a NO conversion of less than 12%. This temperature/conversion regime represents the parameter space in which we can very accurately determine the specific rates of the reaction. However, because it has been reported that N_2O selectivity falls dramatically at high temperatures and/or high NO conversions, we decided to explore the high-temperature/conversion regime. It should be noted that under these reaction conditions the reaction ran too fast for us to accurately determine the specific rates; i.e., reaction times in our batch reactor are less than 10 sec. We believe, however, that the reaction rate is not mass transfer limited in this high-temperature regime since the TONs continue to increase as the temperature is increased. Although we cannot accurately determine the absolute reaction rates, we can still accurately measure the N_2O selectivity. In Fig. 5 we show the effect of temperature on N_2O selectivity using three different gas mixtures: 8 Torr NO/40 Torr CO (8/40), 8 Torr NO/8 Torr CO (8/8), and 40 Torr NO/8 Torr CO (40/8). Conversion of NO is kept below 20% in these experiments to minimize possible complications from conversion effects. At temperatures below 648 K, the selectivity toward N_2O ranges between 73 and 82%, with an average selectivity of around 78% for all reactant mixtures. However, at temperatures above 648 K, the selectivity of N_2O is a strong function of temperature and this temperature-dependent selectivity is also a strong function of the reactant mixture employed. The data of Fig. 5 show that N_2O selectivity decreases significantly from 74% (648 K) to 24% (823 K) for the 8/40 sample, while the N_2O selectivity for the 8/8 mixture decreases from 79% (648 K) to 33% (823 K). For a higher NO pressure (40/8), the selectivity for N_2O decreases more modestly from 76% (623 K) to 54% (873 K).

As described in Section 2.4, there is a short heating and cooling cycle in our reactor that may contribute reaction products that are formed in the ramping up and cooling down cycles. This effect can be significant especially when the reaction time is relatively short. For example, the reaction time is only 1 sec for the data obtained at 823 K to keep the NO conversion low. In order to investigate whether an even higher N_2 selectivity can be obtained, the following experiment was performed: first, the gas manifold was pressurized with the reactant mixture that upon opening the reactor inlet valve, would give an 8/8 mixture in the reactor; second, the crystal was maintained

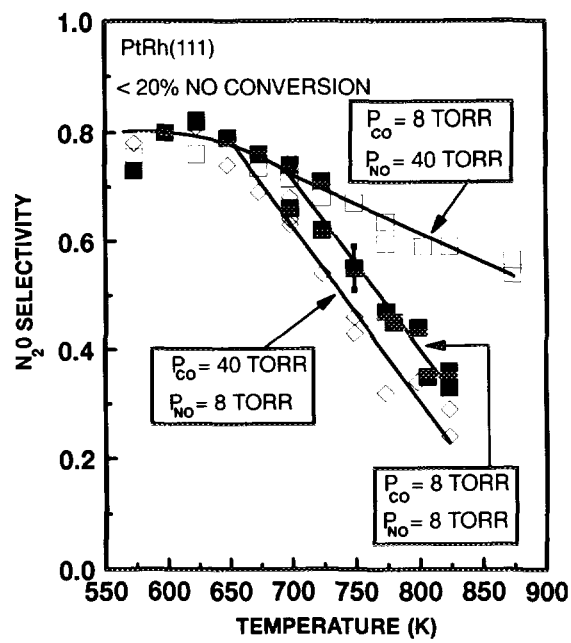

FIG. 5. Effect of temperature on N_2O selectivity for three different reactant mixtures: P_{CO}/P_{NO} = 8/40, 8/8, and 40/8. Conversion of NO was kept below 20%. For all three mixtures the N_2O selectivity drops for temperatures above 700 K.

at 823 K at 10^{-8} Torr vacuum; third, the reactor inlet valve was then quickly opened and closed to fill the reactor; fourth, the reactor outlet valve to the GC sample loop was quickly opened to obtain a sample. In this way, the reactant mixture did not go through a heating and cooling period. Indeed, by using this approach, the selectivity of N_2O from an 8/8 mixture can be further pushed down to 22 from 33% at a comparable NO conversion. It should be noted that in other cases when the reaction time is on the order of minutes, the contributions from the heating and cooling period have been determined to be insignificant.

In order to probe the effect of the amount of N_2O built up in the gas phase on the N_2O selectivity, we performed the experiment shown in Fig. 6. In Fig. 6 we plot the N_2O selectivity vs the amount of NO converted into product for reactions of three different mixtures of NO–CO: 8/8, 40/8, and 8/40. The reaction was run at 698 K. For the 8/8 mixture, the N_2O selectivity decreases from 76 to 63% as the first 6 Torr of the NO is consumed; however, as the last 2 Torr of NO is consumed the N_2O selectivity drops much more sharply, falling below 50%. In a companion experiment the same reaction was next run with a 40/8 mixture. In this experiment we are able to convert the same amount of NO into N_2O and N_2 without drastically altering the gas-phase NO pressure. As Fig. 6 shows, under conditions where the total NO conversion is low

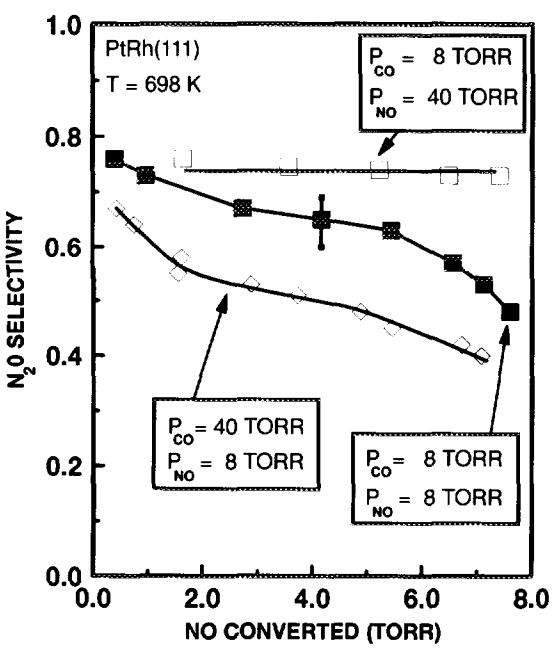

FIG. 6. Effect of NO converted (in Torr) on N_2O selectivity for three different reactant mixtures: P_{CO}/P_{NO} = 8/40, 8/8, and 40/8. At high P_{CO}/P_{NO} ratios the N_2O selectivity is sensitive to the amount of NO remaining in the gas phase.

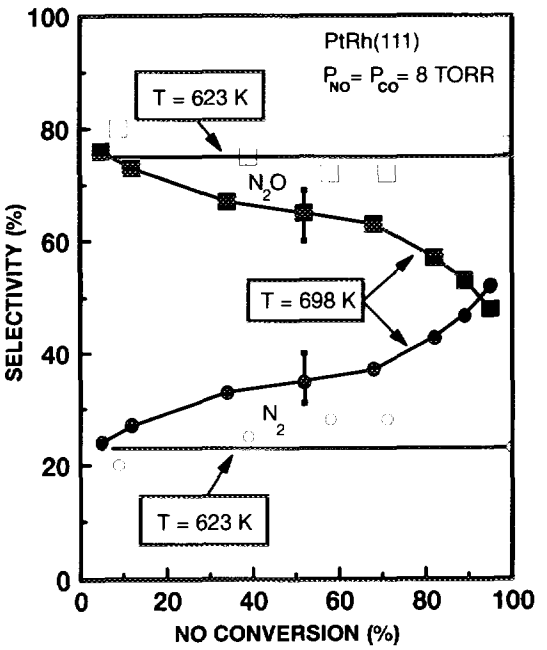

FIG. 7. Effect of NO conversion on N_2O selectivity at 623 and 698 K. Note that at 623 K there is no significant change in selectivity even at high NO conversion.

(<20%) the same number of NO molecules can be converted into product without significantly changing the N_2O selectivity from its initial value of 76%. On the other hand, the 8/40 mixture shows a trend similar to that of the 8/8 mixture, except that the selectivities are lower by 10–20% throughout the conversion range.

Figure 7 addresses a different question: what is the effect of temperature at high NO conversions? To address this question the N_2O selectivity was measured over a wide range of NO conversions at two different temperatures. What Fig. 7 shows is that provided the reaction temperature is 623 K or below, running the reaction to very high NO conversions has virtually no effect on the N_2O selectivity: it remains near 76%. However, if the reaction is run 75 K higher, then the selectivity behavior is quite different. As Fig. 7 shows for the data obtained at 698 K the N_2O selectivity falls from its low NO conversion value of 78% to about 50% by the time 90% of the NO in the reactor is consumed.

In a final experiment we assessed the feasibility that gas-phase N_2O could readsorb and react further to make N_2. In this experiment we measured the N_2 TON at 698 K for a mixture with 8/8 with varying amounts of added N_2O (0.5 to 80 Torr). We focused on the N_2 TONs because very large amounts of added N_2O made it difficult to account for the N_2O formed accurately. For the 10 different N_2O pressures we explored, we found no evidence that the N_2O that we added to the gas phase

was reacting to form N_2. This statement is based on our observation that the N_2 TONs with N_2O added were unchanged from those observed without any added gas-phase N_2O.

4. DISCUSSION

4.1. Reaction Kinetics of $Pt_{10}Rh_{90}(111)$

N_2O is the undesirable product of the NO–CO reaction because of its importance as a "greenhouse" gas; therefore, the selectivity for N_2 versus N_2O is the aspect of the NO–CO reaction of the most practical importance. It is also true that the selectivity for N_2O poses some very interesting fundamental questions because of the very rich N_2O formation kinetics exhibited by Rh and Pt–Rh catalysts. It is well known from laboratory studies that N_2O is the major product of the reaction at low temperatures and/or low NO conversions, but that only N_2 is formed at higher temperatures and/or higher NO conversions (15–18). This transition from N_2O formation to N_2 formation is typically observed for supported catalysts in flow reactors as the catalyst goes through "light-off"—light-off is defined as the temperature for 50% NO conversion. Perhaps the primary experimental advantage that the experiments we present here have is that our experiments were conducted in a batch reactor. Although this reactor design has some limitations, one advantage of a batch reactor is that it is trivial to decouple two important variables, those being reaction temperature and reactant conversion.

4.1.1. Low-temperature (<700 K) behavior. In this section we discuss the kinetic behavior of the $Pt_{10}Rh_{90}(111)$ catalyst at temperatures below 700 K, where we observe that the NO–CO reaction is remarkably insensitive to reaction conditions of the gas-phase composition, reaction temperature, and NO conversion. With regard to gas-phase pressures, Figs. 3 and 4 show that the TONs for all three products are independent of both NO and CO pressure (between 2 and 40 Torr); therefore, the reaction is zero order in both NO and CO pressure. With regard to reaction temperature, in Fig. 1 and Table 1 we show that the E_a for formation of all three products is the same, 32 kcal/mol, within experimental error. Thus, as temperature is varied there is no change in the selectivity for the reaction. This point is also made strongly in Fig. 5, which shows that this temperature insensitivity holds for a wide range of different gas-phase compositions. With regard to NO conversion, Fig. 7 shows that at 623 K the selectivity does not depend on the percent NO conversion. However, at 698 K, the upper limit of the low-temperature region, we do see that as we approach 100% NO conversion the reaction starts to produce more N_2 than N_2O. We consider these data (698 K) in the next section.

How do we explain the remarkable insensitivity of the NO–CO reaction to reaction conditions in this low-temperature regime? Looking first at the pressure dependence, the first and most obvious inference of the zero-order reaction kinetics is that changes in the gas-phase composition do not result in significant changes in the surface coverages of the reactants (NO, N, CO, O). Within our temperature and pressure range, there is only one reasonable explanation for why the surface coverage is independent of the gas-phase pressures: the surface is either saturated with or very near saturated at the sites where the NO and CO *initially adsorb*. It is our view that NO and CO, which adsorb in atop or bridging sites (22, 23), are not in direct site competition with N and O, which are known to adsorb in the threefold hollow sites (22, 23). Thus, it is not a requirement that the hollow sites be saturated but merely that the atop and bridging sites be *effectively* saturated. By effectively saturated we mean that either all atop and bridging sites are full or that the NO and CO sticking coefficients are very low for the few sites that remain on the surface. We bring up this sticking coefficient argument because it is known that CO and NO adsorb via a mobile precursor (30), which means that the sticking coefficient falls sharply as the surface coverage nears saturation, making it increasingly more difficult to fill the last sites on the surface (31). Thus for temperatures below 700 K the surface is effectively full of adsorbates in the atop and bridging sites and as a consequence, varying the NO and CO pressures has no effect on the reaction rate or selectivity. Postreaction XPS analysis suggests that the surface is NO covered; however, this type of *ex situ* analysis can be flawed if during sample cooling and reactor evacuation a significant amount of desorption occurs. Considering how strongly NO and CO are adsorbed on Rh, we feel that the postreaction analysis is qualitatively correct in suggesting that the surface is largely NO covered during the reaction.

In the preceding paragraph we make the point that the pressure independence of the activity results from the fact that the surface is effectively full of NO. Why then is the N_2O selectivity insensitive to reaction temperature? One would think that as the temperature is raised reaction and/or desorption would tend to clean up the surface, leading to surface coverage changes. However, this is not the case when the flux of reactants to the surface is sufficiently high so as to dominate any increases in reaction rates obtained by increasing the temperature (E_a is about 32 kcal/mol). We believe that for NO pressures above 2 Torr and temperatures between 500 and 700 K changes in surface temperature do not significantly affect the surface coverages of NO, N, CO, and O. Thus, in

this temperature and pressure regime the selectivity and reaction orders do not change significantly with temperature.

4.1.2. High-temperature (>700 K) behavior. At temperatures near or above 700 K the kinetic behavior of the $Pt_{10}Rh_{90}(111)$ starts to change from that observed at lower temperature. This change is marked primarily by the fact that the N_2O selectivity is strongly dependent on the reaction temperature, the gas-phase composition, and the percent NO conversion. For all three gas mixtures examined in Fig. 5, raising the temperature decreases the N_2O selectivity. This means that E_a is no longer the same for both N_2 and N_2O formation as it was at lower temperatures. Also, the fact that gas-phase composition affects the selectivity (Fig. 5) means that the reaction is no longer zero order in either NO or CO pressure. This change in pressure dependence from zero-order to nonzero-order kinetics can only mean that above 650–700 K the surface coverages are no longer stable and therefore probably not saturated. In other words, the surface coverages are now changing with reaction conditions, and this gives us a powerful handle on the reaction mechanism.

The effect of reaction temperature on the N_2O selectivity is examined in Figs. 5 and 7. The data of Fig. 5 show that as the temperature is raised above 700 K, the selectivity for N_2O begins to fall. The details of this selectivity decrease (Fig. 5) are strongly dependent on the NO and CO pressures; but, in all cases the amount of N_2O produced (relative to N_2) falls as the temperature is increased. As for reactant pressures, the data of Figs. 5 and 6 best address the effect of reactant pressure on the N_2O selectivity above 700 K. At elevated temperatures (say 800 K) changing either NO or CO pressure has an effect on the selectivity for N_2O. As shown in Fig. 5, increasing the NO pressure from 8 to 40 Torr increases the N_2O selectivity from 45 to 60% (800 K). Figure 6 shows that the effect of reactant pressures holds for virtually any NO conversion. Since the selectivity is changing as the NO or CO pressure is raised, we know that the surface coverages must be changing in response to these gas-phase pressure changes. The primary effect on the surface of increasing the NO pressure must be to increase the NO coverage, which in turn increases the N_2O selectivity. Increasing the CO pressure from 8 to 40 Torr (Fig. 5, 800 K) affects the selectivity for N_2O but not nearly as much as increasing the NO pressure. Increasing the CO pressure reduces the NO coverage somewhat, while increasing the NO pressure increases the NO coverage more, thus enhancing N_2O selectivity. This is consistent with postreaction analysis of the surface, which suggests that CO coverages are small under all conditions. Therefore, changes in CO coverage lead to rather small changes in selectivity.

The final effect to discuss is the effect of NO conversion on N_2O selectivity. Figures 6 and 7 address this point in two different ways. In Fig. 7 we show that, provided the temperature is around 700 K, running the reaction very near to completion has the effect of lowering the N_2O selectivity. Although the effect is not very large, keep in mind that in this batch reactor the selectivity measured at 95% conversion reflects the integral of the selectivities over all conversions up to that point. Since the selectivity is relatively stable at about 65–75% up to 65% conversion, as the last 30% of the NO is reacted (Fig. 7) the selectivity must then be quite low in order to lower the integrated selectivity to below 50%. We calculate that for NO conversions above 65% the selectivity of N_2O is only about 20%. We conducted measurements as a function of NO conversion, primarily because this is a very commonly observed quantity in flow reactors; however, in actuality our experiment changes two variables at once: it decreases the pressures of the reactants (NO and CO) and it increases the pressures of the products (N_2O, N_2, CO_2). Provided that readsorption and further reaction of the products are negligible, product generation is not a problem. However, for the NO–CO reaction there is some question of whether N_2O readsorption and reaction are important (16). In order to address whether reactant removal or product generation is more important for controlling the selectivity at high NO conversions, we performed the experiment in Fig. 6. In this experiment we used three different gas mixtures and ran the reaction for various times at 698 K. The x axis of Fig. 6 is *not* percent NO conversion, as is typically plotted, but instead gives the amount of NO (in Torr) converted to product. Thus, for the case with 40 Torr NO the overall NO conversion is very low, although the amount of NO reacted is the same as for the 8-Torr case where the NO conversion is quite high. These data strongly suggest that product generation at high NO conversions is not the important parameter in determining the N_2O selectivity. Instead, they support the data of Fig. 5 in that they show that lowering the gas-phase NO pressure (or raising CO pressure) is the more important factor in determining the N_2O selectivity. Both of these pressure effects should give the same surface coverage effect, namely a lowering of the surface NO concentration. The study of the effect of N_2O addition on an 8/8 mixture futher supports this point, since no changes in selectivity were observed over a wide range of N_2O pressures added.

4.1.3. Summary: $Pt_{10}Rh_{90}(111)$ NO–CO kinetics. In Section 4.1.1 we discussed how the activity and selectivity respond to changes in the reaction conditions. In this section we give our view of how the surface response to those changes and how that explains the observed activity

and selectivity. It is our view that any valid mechanism must be supported by modeling to show that it can *quantitatively* describe the observed reaction kinetics. However, we feel that it is useful to give our view of how the NO–CO reaction runs on this surface. In our opinion the low-temperature kinetic data presented in Figs. 1–5 are consistent with the following picture. The NO–CO reaction rate and selectivity are controlled by the NO adsorption/desorption equilibrium, a fact previously recognized by Oh and Carpenter (32). As a result of relatively slow NO desorption and a high NO sticking coefficient, the surface is effectively full of NO. The most important effect of having this very high NO coverage is that it tends to choke off NO dissociation. The fact that adsorbed NO strongly inhibits NO dissociation (21, 24) is well known. Thus, under reaction conditions the NO dissociation rate, which is extremely fast at low coverage (22), is slowed significantly by the presence of neighboring NO molecules. Hence, this inhibition of NO dissociation by adsorbed NO is what controls the delivery rate of N and O to the formation of products. Changes in the reaction temperature and reactant pressures have little effect on the surface coverages of NO, N, O, and CO precisely because the surface is effectively full of NO (above 2 Torr NO and below 700 K) and the NO flux is high compared to the desorption rate for NO. For this reason the selectivity and overall activity of the surface are insensitive to gas-phase presssure (above 2 Torr). We suggest that even greater insight into this reaction can be obtained by examining the reaction at pressures below 2 Torr of NO. As the pressure is lowered one should observe the transition from zero-order to nonzero-order kinetics with rates limited by the availability of NO. Unfortunately, we were experimentally unable to obtain data at these lower pressures.

Our results at higher temperatures give us good insight into the most interesting aspect of the NO–CO reaction over Rh-containing catalysts: the selectivity for N_2O. By taking advantage of the unique properties of our batch reactor system, we have been able to decouple the reaction temperature from the NO conversion. These quantities typically go hand-in-hand in most of the reported supported catalyst data in flow reactors. Our results show that both high-temperature and high-NO conversions work in concert to effect a lowering in the selectivity for N_2O. We conclude that the important gas-phase phenomenon that occurs at high-NO conversions is a lowering of the NO pressure. The most important surface phenomenon that occurs at high temperature is an increase in the NO desorption rate. Both of these effects (lower NO pressure and higher surface temperature) act to shift the NO adsorption/desorption equilibrium so as to lower the surface NO coverage. We speculate that the most important result of lowering the NO coverage is to accelerate the NO dissociation reaction. It is well known from NO TPD experiments that high NO coverages prevent NO dissociation at temperatures that are sufficiently high to completely dissociate lower NO coverages (21, 24). We speculate that as the NO coverage falls, the N_2O selectivity drops because of a sharp increase in the amount of N_2 formed, not a sharp decline in the N_2O formation rate. This speculation is based on new measurements of N + N reaction rates by Belton *et al.* (33) over Rh(111). In that paper, the authors showed that the N + N recombination rate is extremely sensitive to N coverage, with the reaction rates changing by about 4 orders of magnitude between low and high coverage. It is this strong coverage dependence in the N + N rate that we believe is important for decreasing the selectivity for N_2O.

4.2. *Comparison of $Pt_{10}Rh_{90}(111)$ Kinetics with those of Other Systems*

4.2.1. Comparison with NO–CO over Rh(111). One of the goals of this study is to examine the effect of adding Pt to a Rh surface. Under the conditions of these experiments the $Pt_{10}Rh_{90}(111)$ surface has about 30% Pt and 70% Rh at the surface (see Section 2.6). Our results show that when compared in the same temperature range (573 to 648 K), $Pt_{10}Rh_{90}(111)$ and Rh(111) (10) have almost the same NO–CO activity. We make five comparisons of the NO–CO activity of $Pt_{10}Rh_{90}(111)$ and Rh(111) in this paper. First, the reaction products are the same for both surfaces: N_2, N_2C, and CO_2. Second, N_2O selectivity is very similar, being between 70 and 80% N_2O below 650 K. Third, the NO–CO reaction is roughly zero order (Figs. 3 and 4) in both CO and NO pressure for formation of all three products over the pressure range we examined. Fourth, the activation energies for formation of N_2, N_2O, and CO_2, (Fig. 2 and Table 1) are very similar: all are around 32 kcal/mol. Fifth, the TONs for N_2, N_2O, and CO_2 formation (Fig. 2) are slightly lower for $Pt_{10}Rh_{90}(111)$ than for Rh(111). We find that the reaction runs between 35 and 50% slower (CO_2 molecules *surface site*$^{-1}$ *sec*$^{-1}$) on the $Pt_{10}Rh_{90}(111)$ surface. Perhaps a better way to look at the data is to calculate the rate *per surface Rh atom* instead of per surface atom (Pt and Rh). On a per Rh atom basis the TONs are the same, within experimental error, for the two surfaces. Based on this TON comparison we conclude that there is no evidence for any Pt–Rh synergism or strong poisoning of the NO–CO reaction within the temperature and pressure range where both have been investigated. The simplest way to view the activity of the $Pt_{10}Rh_{90}(111)$ surface is to conclude that the surface Pt atoms merely dilute the surface Rh concentration and lower the activity as inert site blockers. Alter-

natively, it could also be the case that all the atoms are active with averaged properties of Pt and Rh. There is no way to distinguish these possibilities based on our data. However, UHV measurements of the NO dissociation rate on the Pt–Rh alloy surface give the activation energy for NO dissociation intermediate between that for NO dissociation on Rh(111) and Pt(111) (6), suggesting the possibility of electronic "averaging."

4.2.2. Comparison of $Pt_{10}Rh_{90}(111)$ to other Pt–Rh single crystal studies. To our knowledge, the data we present here represent the first direct comparison of $Pt_{10}Rh_{90}(111)$ and Rh(111) single crystals for the NO–CO reaction at moderate pressures. There have been other studies using several crystal planes of Pt–Rh alloy for NO–CO in the 10^{-7} mbar range (27, 28) and Pt–Rh(100) surface for NO–H_2 reaction in the 10^{-7} mbar and 10 mbar range (29). For the NO–CO study, the reaction rate increases in the order Pt–Rh (111) > (100) > (410) > (210). However, there was no measurable difference when the surface composition of Pt–Rh(111) was changed from 25 to 45% Pt. Thus, we are confident that the differences in selectivity and activity observed are not due to small changes in surface composition during reaction. Contrary to our work, no N_2O formation was reported, probably because of the low reactant partial pressures employed. As discussed in later sections, N_2O formation requires a high concentration of both N_a and NO_a. Though NO–H_2 is a different reaction from NO–CO, there is an interesting analogy to the formation of N_2O. First, the amount of N_2O formed increased with NO partial pressure; second, the N_2O formed decreases with increasing temperature. This trend is consistent with what we observe for the NO–CO reaction. It should be noted that in that study (29), N_2O is a very minor product in the 10^{-7} mbar regime.

4.2.3. Comparison of $Pt_{10}Rh_{90}(111)$ and supported Pt–Rh. In a recent study by Leclercq *et al* (7), the effect of Rh addition on the NO–CO activity and selectivity of a Pt/Al_2O_3 catalyst was reported. The catalyst was a 1% Pt–0.2% Rh/Al_2O_3 catalyst, and the reaction mixture is 0.5 mol% CO and 0.56 mol% NO in helium. The S_{N_2O} is around 90% at 433 K, decreases gradually to 50% at 563 K, and then sharply drops to 0% N_2O within the next 30 K. The shape of the selectivity-temperature curve is remarkably similar to our single-crystal data. However, the temperature is shifted by about 150 K. This can be attributed to local heating effects or to differences in crystallographic planes of the supported catalyst particles. Unfortunately, TONs were not reported to allow a direct comparison with our kinetic data. Nevertheless, the similarity in the N_2O selectivity-temperature curves suggests that the supported Pt–Rh catalyst mimics the behavior of a Pt–Rh single crystal.

4.3. Mechanistic Considerations

4.3.1. Previously proposed mechanisms. The mechanism of the NO–CO reaction over Pt–Rh single crystals has not been discussed in detail in previous papers. However, as we show here the activity of this crystal is virtually indistinguishable (within the parameter space for which both have been studied) from that for Rh(111) and supported Rh catalysts. For this reason it is safe to assume that the mechanism for reaction over this alloy is the same as that for the Rh only surface. This assumption is consistent with our conclusion that the Pt surface atoms do not considerably perturb the activity of the Rh atoms.

Several different reaction mechanisms for the NO–CO (9, 13, 15, 17, 34, 36) reaction have been put forth over the years. For completeness and ease of subsequent discussion we simply list all of the reaction steps that have been proposed as part of NO reduction mechanisms. They are:

$$CO_g + S \leftrightarrow CO_a \quad [1]$$

$$NO_g + S \leftrightarrow NO_a \quad [2]$$

$$NO_a + S \rightarrow N_a + O_a \quad [3]$$

$$CO_a + O_a \rightarrow CO_{2g} + 2S \quad [4]$$

$$NO_a + N_a \rightarrow N_2O_a + S \quad [5]$$

$$NO_a + N_a \rightarrow N_{2g} + O_a + S \quad [6]$$

$$N_2O_a \rightarrow N_2O_g + S \quad [7]$$

$$N_2O_a \rightarrow N_{2g} + O_a \quad [8]$$

$$N_a + N_a \rightarrow N_{2g} + 2S. \quad [9]$$

As stated above, the important issue with regard to this reaction is the selectivity for N_2O. There are basically two different ideas as to how the reaction proceeds and therefore how the selectivity is controlled.

In one scheme, proposed for supported Rh catalysts, both N_2O and N_2, at least at low temperature, come from a common intermediate which forms by reaction of NO and N (13, 15, 17, 34, 36). Within the context of this mechanism the selectivity is controlled by the relative rates of disproportionation to give N_2 and desorption to give N_2O from this intermediate. In the case where these ideas were applied to explain the selectivity transition (from N_2O formation to N_2 formation) at "light-off," it was assumed that N_2O disproportionation became much more important at those temperatures and or conversions. A second mechanism in the literature is one that was formulated to explain the activity over both single-crystal Rh and supported Rh catalysts (9). This second mechanism differs from the first primarily in that it has N_2 formed

by two different pathways: NO + N → N_2 at low temperatures and N + N at high temperatures. This second mechanism has NO dissociation being a very fast reaction and thus N atom removal as the rate-limiting step. This mechanism did not include a step for N_2O formation and thus did not address the N_2O selectivity issues.

4.3.2. Pertinent UHV measurements of elementary steps. Most, if not all, of the ambiguities about the mechanism for the NO–CO reaction over Rh and by extension over Pt–Rh are due to uncertainties in the rates of the elementary reaction steps. One of the biggest problems is centered around the rate for the N + N reaction. Exactly what rate constant was employed for this reaction determines whether it can contribute to product generation. Recently Belton *et al.* (33) made some new measurements of the N + N reaction rate over Rh(111) in a UHV study. The most important result of that paper was that the reaction N + N → N_2, which was previously thought to be rather slow, can in fact be as much as 100 times faster than the N_2 formation rates reported in this paper (Fig. 1). This result is critical in that it points out that N + N is certainly fast enough to account for the N_2 formed at higher pressures. These results show that N atom removal is not *inherently* (meaning regardless of the N coverage) the rate-limiting step in the reaction. A second and equally important result of that paper is the observation that the N atom recombination rate is very strongly dependent on N atom coverage. In their paper, Belton *et al.* report that the reaction rate can vary by as much as 10,000 times between low and high N atom coverages. As a result, very small changes in N coverage give very large differences in the N_2 formation rates.

In a second study, Belton *et al.* (35) looked at the reaction of isotopic mixtures of NO and N on Rh(111). The purpose of those experiments was to determine the products of the N + NO reaction, basically to probe reactions [5] and [6] above. Those results showed no evidence for a NO + N → N_2 reaction; however, we did observe the formation of N_2O via NO + N → N_2O. Although these results do not prove that the NO + N → N_2 reaction does not occur, our measurements of both NO + N and N + N reactions show that the simplest plausible explanation is that NO + N forms N_2O, and N_2 comes from N + N. Based on these new elementary step measurements, together with the experimental evidence obtained in this study, we propose that the following mechanism should be used to describe the NO + CO reaction:

$$CO_g + S \leftrightarrow CO_a \quad [1a]$$

$$NO_g + S \leftrightarrow NO_a \quad [2a]$$

$$NO_a + S \rightarrow N_a + O_a \quad [3a]$$

$$CO_a + O_a \rightarrow CO_{2g} + 2S \quad [4a]$$

$$NO_a + N_a \rightarrow N_2O_g + S \quad [5a]$$

$$N_a + N_a \rightarrow N_{2g} + 2S. \quad [6a]$$

4.4. Implications to N_2O Selectivity on Supported Catalysts

The results of this study can shed some light on the understanding of the light-off phenomena observed in supported catalysts. For low loaded Rh/Al_2O_3 catalysts, "light-off" is characterized by a sharp increase in the NO conversion, which is accompanied by a sharp decrease in the N_2O selectivity (15–18). Further, in data taken for actual engine exhaust it has been shown that N_2O emissions are very small under all operating conditions. (8). Our single-crystal catalyst appears to undergo the transition from high N_2O production to N_2 production more slowly than do supported catalysts. We believe this difference in the behaviors of supported and single-crystal catalysts is partially attributable to heat- and mass-transfer effects. We base this conclusion on two observations. First, when NO and CO are reacted over supported catalysts a very large exotherm is generated when the catalyst "lights-off," which results in a very sharp temperature rise in the catalyst bed (100 K/sec for supported catalysts in our reactor). For single crystals, this sharp temperature rise is not obtainable. It appears that for the single crystals heat conduction is relatively rapid compared to the rate of heat release (controlled by the number of Rh surface atoms) and thus no large change in catalyst temperature occurs at light-off. It is our belief that the large reaction exotherm over supported catalysts (which is not present for single crystals) gives rise to two effects. We suspect that the catalyst temperature deviates from the gas-phase temperature (which is typically measured for flow reactors with supported catalysts), leading to ambiguities as to the true particle surface or reaction temperature. Also, it is possible that at these high surface temperatures the reaction becomes so fast that it becomes diffusion limited. Hence, the NO arrival rate at the surface is slow compared to the reaction rate, and thus NO coverages are low, leading to high selectivity for N_2. In our batch reactor we observe that after light-off, supported catalysts are in fact operating diffusion limited (reaction rate is independent of catalyst temperature). It is our belief that these two effects (particle temperatures in excess of gas-phase temperatures and limited diffusion into the catalyst pores) contribute to sharpen the selectivity transition at light-off primarily by lowering the surface NO coverage. Thus it is our opinion that heat- and mass-transfer effects account for some of the differences in the temperature dependence of the N_2O selectivity. However, in some recent experiments over Rh single crystals (37), we have shown that

the N_2O selectivity is sensitive to surface structure. In those experiments, a more open (110) surface made more N_2 and less N_2O than did the close-packed (111) surface. Based on these results it seems likely that particle size effects could account for some of the differences observed for different types of catalysts.

5. CONCLUSIONS

We have studied the effects of temperature, NO conversion, and NO–CO ratio on the activity and selectivity of the NO–CO reaction over a $Pt_{10}Rh_{90}(111)$ surface. The NO–CO activity over the $Pt_{10}Rh_{90}(111)$ is very similar to that over the Rh(111) surface from 573 to 648 K in that both surfaces have the same E_a, reaction orders, products, and selectivities. The TONs for the $Pt_{10}Rh_{90}(111)$ alloy are slightly lower than those for Rh(111), when compared on a *per surface atom* basis; however, the rates per surface Rh atom are virtually unchanged. This behavior gives the appearance of simple dilution by Pt of the Rh surface atom concentration; however, an averaged electronic effect would also be consistent with the data. We have additional evidence supporting electronic effects: the fact that higher rates are seen for the $CO–O_2$ reaction (12). The surface composition remains essentially unchanged over the range of reaction conditions that we explored; however, we did not go extremely oxidizing, which is the condition known to have the largest effect on the surface composition. The $Pt_{10}Rh_{90}(111)$ single crystal mimics the behavior of supported Pt–Rh catalysts in that both show high (~75%) selectivity for N_2O at low temperature, low conversion, or high NO–CO ratio and low or zero N_2O production at high temperature and high NO conversion. Our conclusion is that the N_2O selectivity and the overall reaction rate are controlled by the NO adsorption/desorption equilibrium. Adsorbed NO strongly inhibits the NO dissociation reaction, keeping surface N coverages low. However, once the temperature is raised or the NO pressure lowered, surface NO coverages fall, accelerating the NO dissociation reaction and likewise increasing the N + N reaction. We conclude that these surface kinetics explain the curious N_2O selectivities observed during light-off of supported catalysts.

ACKNOWLEDGMENTS

The authors thank Se Oh for his helpful discussions. K. Y. S. Ng acknowledges partial financial support from General Motors R&D for his sabbatical leave to perform this research.

REFERENCES

1. Taylor, K. C., *CHEMTECH* **20,** 551 (1990).
2. Taylor, K. C., *Catal. Rev.*, in press, 1993.
3. Kim, S., and D'Aniello Jr., M. J., *Appl. Catal.* **56,** 23, 45 (1989).
4. Beck, D. D., DiMaggio, C. L., and Fisher, G. B., submitted for publication.
5. Fisher, G. B., and DiMaggio, C. L., submitted for publication.
6. DiMaggio, C. L., and Fisher, G. B., submitted for publication.
7. Leclercq, G., Dathy, C., Mabilon, G., and Leclercq, L., *Stud. Surf. Sci. Catal.* **71,** 181 (1991).
8. Prigent, M., and Soete, G. D., SAE Technical Paper Series, Paper No. 890492, 1989.
9. Oh, S. H., Fisher, G. B., Carpenter, J. E., and Goodman, D. W., *J. Catal.* **100,** 360 (1986).
10. Belton, D. N., and Schmieg, S. J., *J. Catal.* **144,** 273 (1993).
11. Belton, D. N., and Schmieg, S. J., *J. Catal.* **138,** 90 (1992).
12. Fisher, G. B., Ng, K. Y. S., Belton, D. N., and Schmieg, S. J., in preparation, 1993.
13. Hecker, W. C., and Bell, A. T., *J. Catal.* **84,** 200 (1983).
14. Hecker, W. C., and Bell, A. T., *J. Catal.* **85,** 389 (1984).
15. Cho, B. K., Shanks, B. H., and Bailey, J. E., *J. Catal.* **115,** 486 (1989).
16. McCabe, R. W., and Wong, C., *J. Catal.* **121,** 422 (1990).
17. Cho, B. K., *J. Catal.* **131,** 74 (1991).
18. Oh, S. H., *J. Catal.* **124,** 477 (1990).
19. van den Bosch-Driebergen, A. G., Kieboom, M. N. H., van Dreumel, A., Wolf, R. M., van Delft, F. C. M. J. M., and Nieuwenhuys, B. E., *Catal. Lett.* **2,** 73, 235 (1989).
20. Oh, S. H., and Carpenter, J. E., *J. Catal.* **98,** 178 (1986).
21. Root, T. W., Schmidt, L. D., and Fisher, G. B., *Surf. Sci.* **134,** 30 (1983).
22. Root, T. W., Fisher, G. B., and Schmidt, L. D., *J. Chem. Phys.* **85,** 4679 (1986).
23. Root, T. W., Fisher, G. B., and Schmidt, L. D., *J. Chem. Phys.* **85,** 4687 (1986).
24. Schwartz, S. B., Fisher, G. B., and Schmidt, L. D., *J. Phys. Chem.* **92,** 389 (1988).
25. Peden, C. H. F., Goodman, D. W., Blair, D. S., Fisher, G. B., Berlowitz, P. J., and Oh, S. H., *J. Phys. Chem.* **92,** 1563 (1988).
26. Hendershot, R. E., and Hansen, R. S., *J. Catal.* **98,** 150 (1986).
27. Wolf, R. M., and Siera, J., van Delft, F. C. M. J. M., and Nieuwenhuys, B. E., *Faraday Discuss. Chem. Soc.* **87,** 275 (1989).
28. Siera, J., Rutten, F., and Nieuwenhuys, B. E., *Catal. Today* **10,** 353 (1991).
29. Hirano, H., Yamada, T., Tanaka, K. I., Siera, J., and Nieuwenhuys, B. E., *Surf. Sci.* **262,** 97 (1992).
30. Comrie, C. M., Weinberg, W. H., and Lambert, R. M., *Surf. Sci.* **57,** 619 (1976).
31. Gasser, R. P. H., and Smith, E. B., *Chem. Phys. Lett.* **1,** 457 (1967).
32. Oh, S. H., and Carpenter, J. E., *J. Catal.* **101,** 114 (1986).
33. Belton, D. N., DiMaggio, C. L., and Ng, K. Y. S., *J. Catal.* **144,** 273 (1993).
34. Cho., B., *J. Catal.* **138,** 255 (1992).
35. Belton, D. N., DiMaggio, C. L., and Ng, K. Y. S., submitted for publication.
36. Chin, A. A., and Bell, A. T., *J. Phys. Chem.* **87,** 3700 (1983).
37. Peden, C. H. F., Belton, D. N., and Schmieg, S. J., in preparation.